CrossMark

REGULAR ARTICLE

A topological analysis of the bonding in [M$_2$(CO)$_{10}$] and [M$_3$(μ-H)$_3$(CO)$_{12}$] complexes (M = Mn, Tc, Re)

Juan F. Van der Maelen[1] · Javier A. Cabeza[2]

Abstract The M–M, M–H, and M–CO bonding interactions existing in the group 7 transition metal carbonyl complexes [M$_2$(CO)$_{10}$] and [M$_3$(μ-H)$_3$(CO)$_{12}$] (M = Mn, Tc, Re) have been theoretically studied under the perspective of the Quantum Theory of Atoms in Molecules (QTAIM). Several local and integral topological properties of the electron density involved in these interactions, as well as the source function (SF) and the electron localization function, have been computed. The results confirm that the metal atoms in the binuclear [M$_2$(CO)$_{10}$] complexes are connected through a localized M–M bond that implicates little electron density (it increases from M = Mn to Tc and Re). On the other hand, such a bonding has not been found in the trinuclear [M$_3$(μ-H)$_3$(CO)$_{12}$] complexes, which, instead, contain a *6c–6e* bonding interaction delocalized over their six-membered M$_3$(μ-H)$_3$ ring, as revealed by the non-negligible non-bonding delocalization indexes. The existence of significant CO to M π-back-donation, slightly higher in the trinuclear clusters than in the binuclear complexes, is indicated by the M···O$_{CO}$ delocalization indexes and SF calculations.

✉ Javier A. Cabeza
jac@uniovi.es

Juan F. Van der Maelen
fvu@uniovi.es

1 Departamento de Química Física y Analítica-CINN, Universidad de Oviedo-CSIC, 33071 Oviedo, Spain

2 Departamento de Química Orgánica e Inorgánica-IUQOEM and Centro de Innovación en Química Avanzada ORFEO-CINQA, Universidad de Oviedo-CSIC, 33071 Oviedo, Spain

1 Introduction

In the last two decades, the analysis of the topology of the electron density, under the perspective of the quantum theory of atoms in molecules (QTAIM) [1–8], has been established as a powerful tool, complementary to the molecular orbital (MO) theory, to analyze chemical bonds. QTAIM studies on systems containing light atoms (periods 1–3 of the periodic table) have allowed the establishment of useful links between bonding modes and topological properties of the electron density (both local and integral) and its Laplacian, from both theoretically and experimentally determined electron densities [9–19]. However, such links cannot be straightforwardly extended to compounds with transition metal (M) atoms since the latter display a different and much narrower spectrum of topological indexes [20–39].

Regarding M–M bonds, although they have been extensively studied (different metals and bond orders) under the perspective of the MO theory [40–62], only a few systematic studies on M–M interactions have hitherto been based on the QTAIM approach [63–93]. These studies have shown that the electron density between metal atoms of unbridged M–M bonds of a low formal bond order (≤1) is clearly smaller than that involved in bonds between lighter nonmetallic atoms, whereas, in several instances, no critical points have been found when the metal atoms are spanned by bridging atoms.
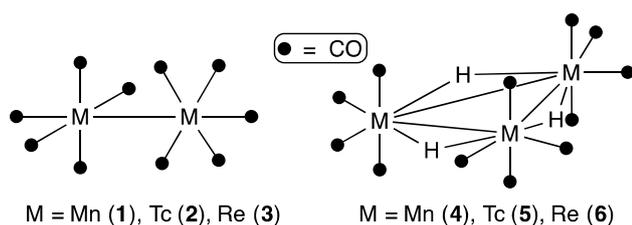
Fig. 1 Schematic structures of the two families of complexes studied in this work

Previous topological studies on complexes containing M–H bonds are very scarce and even rarer are topological studies on di- or polynuclear transition metal complexes containing bridging hydrides. This paper reports the results of an in-depth QTAIM study of the bonding in the group 7 transition metal carbonyl complexes $[M_2(CO)_{10}]$ (M = Mn (**1**), Tc (**2**), Re (**3**)) and $[M_3(\mu\text{-}H)_3(CO)_{12}]$ (M = Mn (**4**), Tc (**5**), Re (**6**) (Fig. 1). We chose these two families of complexes because an analysis of several (local and integral) topological properties of their electron density would allow: (a) to establish the effect of the transition metal atom in the M–M bonding (comparing results of isostructural complexes that only differ in the metal atom) and (b) to determine the effect of the bridging hydrido ligand in the M–M interaction (comparing data of unbridged (**1**–**3**) versus hydride-bridged (**4**–**6**) complexes having the same metal atoms). In addition, this paper also discusses and compares different topological parameters associated with M–CO and M–H bonds for the two families of complexes. To the best of our knowledge, a systematic QTAIM study of isostructural unbridged and ligand-bridged M–M bonded complexes for all the elements of a group of the transition metal series of the periodic table has no precedent in the chemical literature.

2 Computational details

It has been previously shown that the use of relativistic hamiltonians is essential in order to obtain accurate quantitative results from calculations on compounds containing third-row transition metal atoms [64, 94–101], but the effect of using such hamiltonians on calculations involving second-row transition metals is not yet clear. In this work, we decided to use both nonrelativistic and relativistic wavefunctions in all our calculations because this wide approach would provide enough data to unambiguously establish the extent to which the use of nonrelativistic hamiltonians affect QTAIM calculations on isostructural compounds having first-, second-, and third-row transition metals of the same group of the periodic table.

Density functional theory (DFT) computations with nonrelativistic wavefunctions were performed with the GAUSSIAN09 program package [102], using both B3PW91 and B3P86 hybrid functionals in order to check the accuracy of both methods in our calculations [103–105]. The all-electron 6-31G(*d*,*p*) and 6-311++G(3*df*,3*pd*) basis sets were employed for C, H, and O atoms at different steps of the procedure (the former basis set for the geometry optimization processes and the latter for the single-point electronic structure calculations at the optimized geometries), while the LanL2DZ effective core potential and the large all-electron WTBS ('Well-Tempered Basis Set' of Huzinaga and co-workers [106, 107]) basis set were used for Mn, Tc, and Re atoms (again, the former for the geometry optimizations and the latter for the electronic structure calculations).

Computations with relativistic wavefunctions were performed using firstly the scalar ZORA hamiltonian, the PW91 density functional, and the all-electron relativistic QZ4P basis set for all atoms [108], as implemented in the ADF2012 program package [109], in order to obtain relativistically optimized geometries, while the fully relativistic four-component hamiltonian, including spin–orbit terms in double-group symmetry, and the hybrid B1PW91 density functional with relativistic QZ4P basis sets were then used for single-point electronic structure calculations at the optimized geometries.

The previously reported X-ray diffraction structures of $[M_2(CO)_{10}]$ (M = Mn [110], Tc [111], Re [112]) and $[M_3(\mu\text{-}H)_3(CO)_{12}]$ (M = Mn [113], Tc [114], and Re [115]) were used as starting points to calculate optimized geometries. All theoretical models were able to render optimized structures close to the experimental ones, albeit more symmetric, since the binuclear complexes were found to be of exact D_{4d} symmetry (staggered conformation of equatorial CO ligands) and the trinuclear complexes were found to be of exact D_{3h} symmetry (atomic coordinates are available in the Supplementary Information, Tables S1-S6).

The obtained nonrelativistic and relativistic ground-state electronic wavefunctions, which were found to be stable, were then utilized for calculations on the topology of the electron density within the framework of the QTAIM approach. These calculations included both local and integral properties and were carried out with the AIMAll [116], AIM2000 [117], and DGrid [118] programs from GTO- and STO-based wavefunctions. The accuracy of the local properties was 1.0×10^{-10} (from the gradient of the electron density at the bond critical points), whereas that of the integral properties was finally set at least at 1.0×10^{-4} (from the Laplacian of the integrated electron density). Both all-electron nonrelativistic B3P86/6-311++G(3*df*,3*pd*)/WTBS and relativistic SpinOrbit-B1PW91/QZ4P models, applied to the theoretically optimized geometries, were used in all
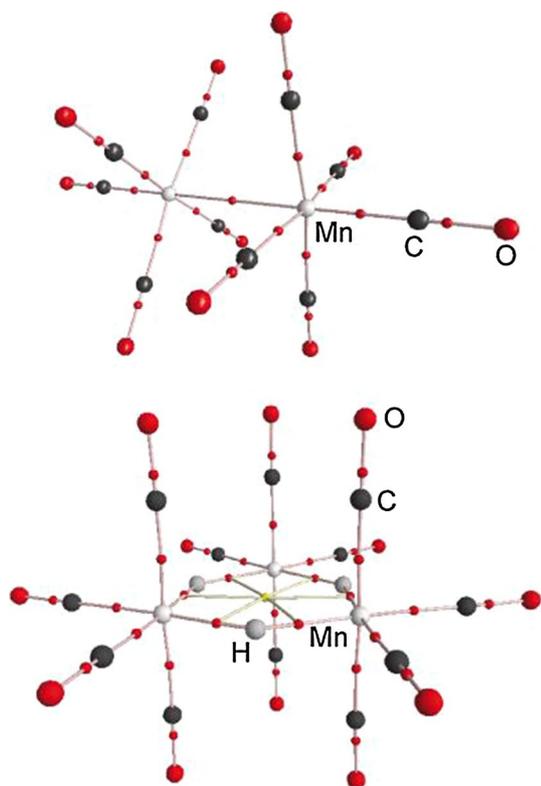
Fig. 2 Topological graphs of compounds **1** (*top*) and **4** (bottom), showing bond paths (*solid beige lines*), ring paths (*solid yellow lines*), and bond (*small red circles*) and ring (*small yellow circles*) critical points

cases to find the critical points. NBO, SF, and ELF analyses were carried out with the program packages, basis sets, and methods already mentioned.

3 Results and discussion

3.1 Critical points and atomic charges

The images shown in Fig. 2 were obtained by applying the QTAIM approach to compounds **1** and **4**. Analogous images corresponding to compounds **2**, **3**, **5**, and **6** are given in the Supplementary Material (Figure S1). They show, along with the atoms corresponding to each complex, the complete set of bond critical points (*bcp*s) and ring critical points (*rcp*s) together with the bond paths (*bp*s) that connect bonded atoms through their corresponding *bcp*s. Concerning M–M interactions, *bp*s and their associated *bcp*s were clearly found in the binuclear complexes (**1**–**3**), with the *bcp*s located exactly at the geometrical center of each M–M vector. On the contrary, no direct *bp*s or *bcp*s were found between the hydride-bridged metal atoms of the trinuclear clusters (**4**–**6**). In regard to M–ligand interactions,
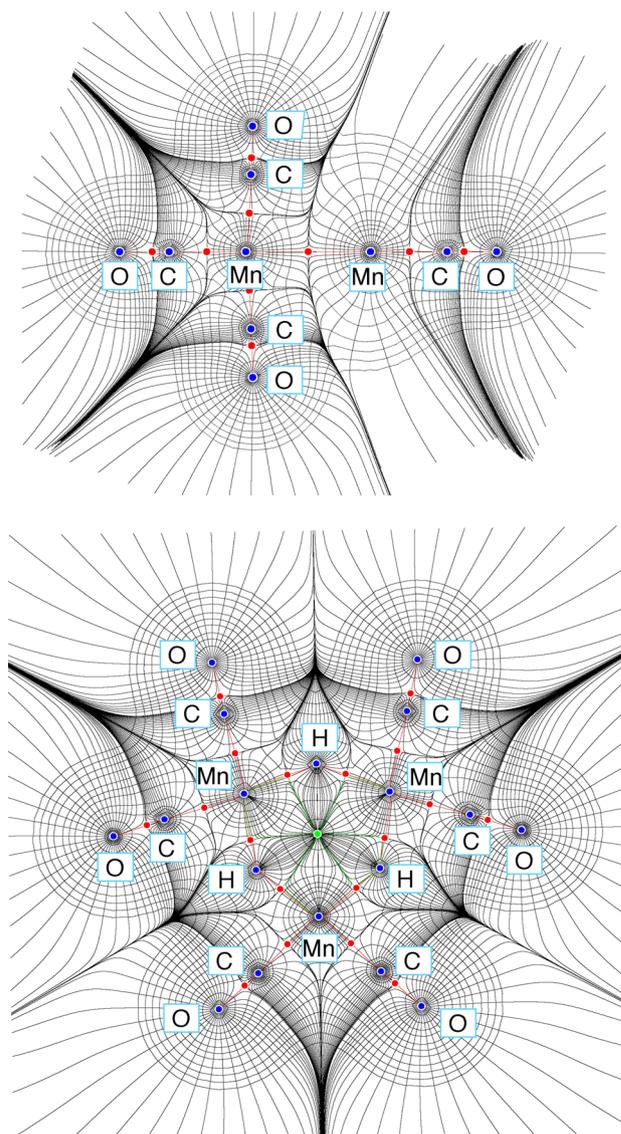
Fig. 3 Gradient trajectories mapped on total electron density plots (contour levels at 0.1 e Å^{-3}) in selected planes containing the metal atoms of compounds **1** (*top*) and **4** (*bottom*), showing the atomic basins, *bp*s (*red lines*), *bcp*s (*red circles*), and a *rcp* (*green circle*)

a *bcp* and a *bp* were found for each of the M–C, M–H, and C–O bonding interactions in all compounds (**1**–**6**), with the *bcp*s located not far from the center of each M–C vector, slightly closer to the H atom in the case of M–H *bcp*s, and clearly closer to the C atom in the case of C–O bonds (the Supplementary Information gives the exact M–*bcp* and *bcp*–B distances of every M–B bond in Table S7). Additionally, a *rcp*, located exactly at the geometrical center of each $M_3(\mu\text{-H})_3$ ring, was obtained for each trinuclear cluster (**4**–**6**).

Figure 3 displays gradient trajectory maps of the total electron density in a Mn_2C_4 plane of complex **1** and in the

Table 1 Atomic charges, $Q(A)$ (e) for selected atoms of complexes **1–6**

Method	Atom	1	2	3	4	5	6
QTAIM	M[a]	0.872	0.953	1.046	0.952	1.060	1.125
	M[b]	0.898	1.003	1.165	0.981	1.058	1.209
	M[c]	0.898	1.003	1.166	0.981	1.058	1.212
	H[a]				–0.322	–0.363	–0.366
	H[b]				–0.324	–0.360	–0.365
	H[c]				–0.324	–0.360	–0.365
Mulliken	M[a]	1.306	1.233	1.301	0.837	0.982	1.046
	M[b]	1.349	1.321	1.415	1.434	1.410	1.443
	M[c]	1.349	1.321	1.422	1.434	1.411	1.452
	H[a]				0.524	0.120	0.065
	H[b]				–0.496	–0.476	–0.442
	H[c]				–0.496	–0.477	–0.444
Multipole	M[b]	1.628	1.691	1.658	2.944	2.900	3.074
	M[c]	1.628	1.692	1.661	2.943	2.900	3.070
	H[b]				–1.543	–1.358	–1.492
	H[c]				–1.544	–1.358	–1.489

[a] Calculated using the nonrelativistic theoretical model B3P86/6-311 ++G(3df,3pd)/WTBS

[b] Calculated using the scalar relativistic theoretical model ZORA-B1PW91/QZ4P

[c] Calculated using the fully relativistic theoretical model SpinOrbit-B1PW91/QZ4P

Mn_3 plane of cluster **4**, showing all *bp*s and *bcp*s, a *rcp*, and the basins of the atoms contained in the chosen planes. As clearly seen in Fig. 3, all *bp*s are straight lines. Analogous images corresponding to compounds **2**, **3**, **5**, and **6** are given in the Supplementary Material. As expected, the maps corresponding to complexes **1–3** are very similar to each other and the same is true for those corresponding to compounds **4–6**.

Integration of the electron density inside each atomic basin rendered the electric charge, $Q(A)$, of each atom (A). Table 1 compares relativistic and nonrelativistic QTAIM charges with those obtained from other commonly used population analysis methods. Whereas Mulliken and 'Multipole' population analyses afforded results rather dependent on the theoretical model used (both method and basis set), the QTAIM approach was very consistent, giving nearly equal values for the charge of each atom regardless of the theoretical model used. In particular, for the Mn complexes **1** and **4**, relativistic and nonrelativistic QTAIM charges calculated using different functionals and basis sets are approximately equal within two significant digits, showing that relativistic effects are unimportant for these first-row transition metal compounds. On the contrary, results for the Tc complexes **2** and **5** are slightly different when using a nonrelativistic approach, although both relativistic treatments (ZORA and SpinOrbit) gave exactly the same results, showing both the small, but admittedly non-negligible, effect that a relativistic treatment has in these second-row transition metal compounds and the versatility

of the scalar (ZORA) approach. On the other hand, for the Re compounds **3** and **6**, charges obtained from both relativistic treatments are not only clearly different from those obtained using nonrelativistic approaches but also different from each other. As expected by symmetry, all metal atoms in each complex (**1–6**) have identical positive charges, ranging from +0.9 e for **1** to +1.2 e for **3** in the binuclear complexes, and from +1.0 e for **4** to +1.2 e for **6** in the trinuclear clusters. Both Mulliken and 'Multipole' population analyses overestimate these charges, while 'Natural Bond Orbital' (NBO) charges (not given in Table 1), calculated using only the nonrelativistic hamiltonian, are closer to the QTAIM charges, with values around +0.7 e and +0.8 e for the metal atoms of the binuclear and trinuclear complexes, respectively. QTAIM charges of the hydrido ligands of **4–6** are negative, ranging from –0.3 e for the hydrides of **4** to –0.4 e for the hydrides of **6**. However, it is noteworthy that the nonrelativistic Mulliken charges of these hydrides are positive, whereas the relativistic ones are negative, even in the first-row transition metal cluster **4**.

Electron configurations of the metal atoms in complexes **1–6**, as obtained from nonrelativistic NBO analyses, are [core]$4s^{0.46} 3d^{5.80}$ (**1**), [core]$5s^{0.45} 4d^{5.83}$ (**2**), [core]$6s^{0.45} 5d^{5.86}$ (**3**), [core]$4s^{0.37} 3d^{5.90}$ (**4**), [core]$5s^{0.39} 4d^{5.87}$ (**5**), and [core]$6s^{0.40} 5d^{5.85}$ (**6**), with other non-core orbitals (Rydberg orbitals) contributing less than 0.1 e.

There are several local (i.e., calculated at the *bcp*) and integral (i.e., calculated over a whole atomic basin, over an interatomic surface, or along a bond path) topological

Table 2 Topological parameters of selected bonds of complexes **1–6**

Bond	Comp.	d (Å)[a]	ρ_b (e Å^{-3})[b]	$\nabla^2\rho_b$ (e Å^{-5})[c]	H_b/ρ_b (h e^{-1})[d]	G_b/ρ_b (h e^{-1})[e]	ε_b[f]	δ(A–B)[g]
M–M	*1*	2.899	0.184	0.182	–0.236	0.305	0.000	0.279
	2	3.070	0.193	0.567	–0.159	0.364	0.000	0.330
	3	3.084	0.212	0.678	–0.175	0.398	0.000	0.338
M–H	*4*	1.699	0.519	4.834	–0.332	0.985	0.063	0.430
	5	1.838	0.513	4.612	–0.303	0.933	0.053	0.473
	6	1.852	0.534	4.371	–0.320	0.893	0.048	0.477
M–C$_{ax}$	*1*	1.780	1.060	12.557	–0.481	1.310	0.000	1.120
	2	1.936	0.957	11.432	–0.423	1.259	0.000	1.152
	3	1.935	1.032	11.763	–0.463	1.261	0.000	1.195
	4	1.797	1.007	13.732	–0.448	1.403	0.008	1.087
	5	1.936	0.918	12.229	–0.391	1.324	0.025	1.126
	6	1.944	0.990	12.537	–0.431	1.318	0.014	1.158
M–C$_{eq}$	*1*	1.835	0.917	12.250	–0.405	1.341	0.006	0.940
	2	1.995	0.811	11.205	–0.336	1.302	0.015	0.960
	3	1.995	0.877	11.767	–0.372	1.311	0.021	0.993
	4	1.843	0.910	13.056	–0.401	1.405	0.015	0.943
	5	1.991	0.811	11.672	–0.329	1.337	0.018	0.960
	6	1.997	0.866	12.127	–0.361	1.341	0.020	0.990

Calculated using the fully relativistic theoretical model SpinOrbit-B1PW91/QZ4P on structures optimized with the scalar relativistic model ZORA-PW91/QZ4P

[a] Bond path length

[b] Electron density at the *bcp*

[c] Laplacian of the electron density at the *bcp*

[d] Total energy density ratio at the *bcp*

[e] Kinetic energy density ratio at the *bcp*

[f] Ellipticity at the *bcp*

[g] Delocalization index

properties of the electron density that have been successfully used to analyze the bonding in compounds containing transition metals. Among the former, the electron density (ρ_b), the ellipticity (ε_b), the Laplacian of the electron density ($\nabla^2\rho_b$), the kinetic energy density ratio (G_b/ρ_b), and the total energy density ratio (H_b/ρ_b, with $H_b(r) = G_b(r) + V_b(r)$ and $\frac{1}{4}\nabla^2\rho_b(r) = 2\,G_b(r) + V_b(r)$, where $V_b(r)$ is the potential energy density) are by far the most common [63–93]. On the other hand, the delocalization index, δ(A–B), which is an integral property, is a useful tool to measure the number of electron pairs delocalized between atoms A and B and can be considered as an estimation of the bond order [12, 20, 80, 85]. Values of these topological properties for selected bonds of complexes **1–6** are given in Table 2.

3.2 M–M interactions in the binuclear complexes 1–3

For the M–M bonds of **1–3**, where a *bcp* has been found between the metal atoms, the small values given in Table 2 for the electron density at the *bcp*s (between 0.18 and 0.21 e Å^{-3}), the small positive values of the Laplacian at

the *bcp*s (between 0.18 and 0.68 e Å^{-5}), the positive but less than unity values of G_b/ρ_b (between 0.31 and 0.40 h e^{-1}), and the small negative values of H_b/ρ_b (between –0.16 and –0.24 h e^{-1}) are typical for open-shell M–M interactions and intermediate between values found for pure covalent and pure ionic bonds between nonmetal atoms. A slight increase in the electron density and also of its Laplacian is observed on going from **1** to **3**. This suggests that the M–M bond strength is greater for Re than for Tc and Mn. The *bp* lengths are very similar to the interatomic distances obtained from both X-ray diffraction data [110–112] and theoretically optimized geometries (see the Supplementary Information, Table S7), with an ellipticity equal to zero in the three cases, indicating straight bonding interactions with a cylindrical topology of the bond at the *bcp*. Rather interestingly, the topological indexes of the M–M bonds of **1–3** are comparable to those previously obtained for [Mn$_2$(CO)$_{10}$] (from both experimental and theoretical electron densities) [29, 82, 110] and for other complexes with an unbridged M–M bond with a formal bond order of about unity, such as [Co$_2$(CO)$_8$] and [Co$_2$(CO)$_6$(AsPh$_3$)$_2$] [20], [Cr$_2$Cp$_2$(CO)$_6$] [67], [Zn$_2$Cp$_2^*$] [23], [Ru$_3$(CO)$_{12}$] [72, 78], and [Os$_3$(CO)$_{12}$]

Table 3 Integrated electron density over the whole interatomic surface, $\int_{M\cap X}\rho$ (e Å^{-1}), for selected bonding interactions of **1–6**

Bond	**1**	**2**	**3**	**4**	**5**	**6**
M–M	1.815	1.662	1.732			
M–H				1.586	1.492	1.598
M–C$_{ax}$	2.481	2.258	2.382	1.989	1.729	1.856
M–C$_{eq}$	2.417	2.223	2.329	1.938	1.711	1.807

Calculation level as in Table 2

[64]. On the other hand, the data given in Table 2 for M–M bonds in **1–3** are considerably different from those previously reported for complexes having M–M bonds of higher formal bond order, for which shorter bp lengths, greater ρ_b, much greater $\nabla^2\rho_b$, and greater $|H_b/\rho_b|$ and G_b/ρ_b have been reported [63–71]. In particular, values listed in Table 2 for $\nabla^2\rho_b$ are approximately between one-third and less than one-tenth times those found for typical M–M multiple bonds. For instance, for the Tc–Tc interaction in [Tc$_2$(μ-HNCHNH)$_4$], which has a formal quadruple bond between the Tc atoms, $\nabla^2\rho_b = 12.088$ e Å^{-5} [63], a value rather similar to those obtained for other binuclear compounds with M–M formal bond orders of three or four, such as [Mo$_2$Cl$_8$]$^{4-}$ [68], [Mo$_2$(μ-CH$_3$CO$_2$)$_2$(μ-Cl)$_2$Cl$_4$]$^{2-}$ [68], [Cr$_2$(μ-η^8-C$_8$H$_8$)Cp$_2$] [67], or [Cr$_2$(μ-η^3-C$_3$H$_5$)$_2$Cp$_2$] [67]. The electron density at the bcp, ρ_b, also increases with the bond order, but it is not as sensitive as its Laplacian in order to discriminate between different bond orders. Additionally, values of H_b/ρ_b and G_b/ρ_b for M–M bonds in **1–3** are farther away from zero than those found for typical M–M multiple bonds.

On the other hand, it is well known that some integral topological properties are more useful than local topological properties for characterizing M–M bonds with transition metals [3, 4, 12]. The delocalization index, δ(A–B), which estimates the number of electron pairs delocalized between atoms A and B, is by far the integral topological property that has been most frequently used in theoretical QTAIM studies [12, 20]. The low δ(M–M) values calculated for **1–3** (between 0.28 for the Mn complex and 0.34 for the Re complex, see Table 2) are comparable to those found for other carbonyl complexes having single M–M bonds, such as [Cr$_2$Cp$_2$(CO)$_6$] (0.27) [67], [Co$_2$(CO)$_6$(AsPh$_3$)$_2$] (0.51) [20], and [Os$_3$(CO)$_{12}$] (0.38) [64], whereas δ(M–M) values found for multiple M–M bonds are always greater than unity [67, 68].

The integrated electron density over the whole interatomic surface, $\int_{A\cap B}\rho$, which is also an integral property, is an additional tool for characterizing bonding interactions since it is related to the bond strength [1, 3, 4, 63], although it has been seldom applied to M–M bonds. The values of $\int_{M\cap M}\rho$ found for **1–3** (in the range 1.73–1.82 e Å^{-1}; Table 3) are only a bit higher than those calculated for M–M bonds in [Zn$_2$Cp$_2$*] (1.25 e Å^{-1}) [23], [Ru$_3$(μ-H)$_2$(μ_3-MeImCH)(CO)$_9$] (1.36 e Å^{-1}) [77], [Os$_3$(CO)$_{12}$],

Table 4 Source function contributions (%) of all atoms to the electron density at the M–M bcp of complexes **1–3**

Atom	**1**	**2**	**3**
M	–28.60	–14.04	–11.52
C$_{ax}$	2.62	1.49	1.81
C$_{eq}$	–1.20	–1.24	–0.31
O$_{ax}$	10.38	8.75	7.91
O$_{eq}$	17.60	14.69	13.26

Calculation level as in Table 2

[Os$_3$(μ-H)$_2$(CO)$_{10}$], [Os$_3$(μ-H)(μ-OH)(CO)$_{10}$], and [Os$_3$(μ-H)(μ-Cl)(CO)$_{10}$] (between 1.44 and 1.52 e Å^{-1}) [64], [Co$_2$(CO)$_8$] (1.56 e Å^{-1}) [20], [Mo$_2$(μ-CH$_3$CO$_2$)$_2$(μ-Cl)$_2$Cl$_4$]$^{2-}$ (1.08 e Å^{-1}) [68], and [Mo$_2$(μ-Cl)$_3$Cl$_6$]$^{3-}$ (1.54 e Å^{-1}) [68].

Another topological property of integral character is the so-called source function, S(A), which estimates the contribution of every atom basin to the electron density localized at any point of the molecule, in particular at any critical point [63, 70]. The contribution (%) of each individual atom in complexes **1–3** to the corresponding M–M bcp is given in Table 4. Interestingly, the major contributions come from the carbonyl O atoms (the equatorial ones contributing more than the axial ones, and those of the Mn complex more than those of Tc and Re complexes). On the other hand, the large negative S(M) values at the M–M bcps indicate that M atoms act as sinks for the electron density, instead as sources. Additionally, the fact that S(M) at the M–M bcp in **1** is more than twice that in **3** is a clear indication that carbonyl ligands are less essential to the M–M bonding in the Re complex than in the Mn complex. As a comparison, for the similar carbonyl complex [Co$_2$(CO)$_8$], S(Co) = –4.4 % at the Co–Co bcp [90].

3.3 M–M and M–H interactions in the trinuclear clusters 4–6

As stated above, no bcp has been found between any pair of metal atoms in compounds **4–6**. Therefore, there is no localized electron density between metal atoms in these clusters.

Table 5 Source function contributions (%) of selected atoms to the electron density at M–H *bcp*s of complexes **4–6**

Atom	4	5	6
M (bond)	16.74	23.84	24.45
M (no bond)	–1.91	–1.31	–1.31
H (bond)	33.51	34.97	34.54
H (no bond)	1.10	1.06	1.11
C_{ax}	2.30	1.70	1.52
C_{eq}	1.38	0.47	0.67
O_{ax}	6.67	5.83	5.56
O_{eq}	7.42	6.48	5.99

Calculation level as in Table 2

Table 6 Delocalization indexes, $\delta(A\cdots B)$, for selected non-bonding $A\cdots B$ interactions of **4–6**

Interaction	4	5	6
$M\cdots M$	0.128	0.134	0.166
$H\cdots H$	0.012	0.008	0.005
$M\cdots H$	0.014	0.013	0.013

Calculation level as in Table 2

Concerning M–H interactions in **4–6**, the values given in Table 2 for the electron density at the M–H *bcp*s (between 0.51 and 0.53 e Å^{-3}), the positive values of the Laplacian at the *bcp*s (between 4.37 and 4.83 e Å^{-5}), the positive and close to unity values of G_b/ρ_b (between 0.89 and 0.98 h e^{-1}), and the negative values of H_b/ρ_b (between –0.30 and –0.33 h e^{-1}) are comparable to that of pure covalent single bonds between nonmetal atoms [1–19]. In addition, the *bp* lengths are similar to the interatomic distances obtained from both X-ray diffraction data [113–115] and the theoretically optimized geometries (see the Supplementary Information, Table S7), with and ellipticity only slightly greater than zero in the three complexes, indicating nearly straight bonding interactions between metal and hydrogen atoms. To the best of our knowledge, previous topological studies on complexes containing M–H bonds on di- or polynuclear transition metal complexes containing bridging hydrides are restricted to just three works that study the complexes $[Cr_2(\mu\text{-}H)(CO)_{10}]^-$ [91], $[Ru_3(\mu\text{-}H)_2(\mu^3\text{-MeImCH})(CO)_9]$ [77], and $[Os_3(\mu\text{-}H)_2(CO)_{10}]$, $[Os_3(\mu\text{-}H)(\mu\text{-OH})(CO)_{10}]$, and $[Os_3(\mu\text{-}H)(\mu\text{-Cl})(CO)_{10}]$ [64]. Table 2 indicates that the $\delta(M\text{–}H)$ delocalization indexes for **4–6** (between 0.430 and 0.477) are comparable to those found for Ru–H (0.474) and Os–H (between 0.426 and 0.449) bonds of the above-mentioned triruthenium and triosmium clusters, while they are higher than those of $[Cr_2(\mu\text{-}H)(CO)_{10}]^-$ (0.38) and only a bit lower than that of the terminal hydrido complex $[CrH(CO)_5]^-$ (0.59). Interestingly, the $\delta(M\text{–}H)$ values of **4–6** suggest that just half an electron pair is shared in each of the six M–H bonds, in spite of the fact that the integrated electron density over the whole interatomic surface for each M–H bond (with values in the range 1.492–1.598 e Å^{-1}, Table 3) confirms that the strength of these bonds is comparable to that of pure covalent single bonds between nonmetal atoms. Table 5 shows SF contributions (%) of selected atoms of complexes **4–6** to their M–H *bcp*s, indicating that the electron density
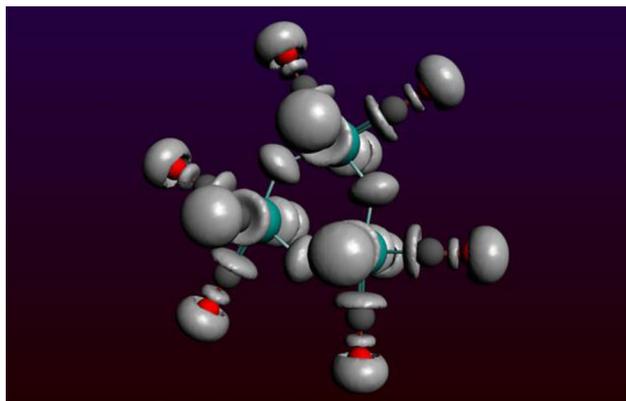
at these points comes mainly from both bonded atoms (between a 50 % for the Mn cluster **4** and a 59 % for the Re cluster **6**), with a non-negligible contribution from the axial and equatorial carbonyl O atoms (ranging from 14 to 12 %, respectively). On the other hand, the remaining two M atoms, not bonded to the corresponding H atom, act as sinks for the electron density, instead as sources, showing small negative contributions of the SF that are similar in the three complexes (between –1.3 and –1.9 % from each M atom, in average), with the other two bridging H atoms almost compensating this behavior, with very small and nearly equal positive contributions (1.1 % from each H atom, in average).

The delocalization indexes of the non-bonding $M\cdots M$, $M\cdots H$, and $H\cdots H$ interactions in complexes **4–6** (Table 6) also contribute to shed some light on the characteristics of these interactions. Although small, they are not negligible at all but comparable in magnitude to, or even greater than, values found for other ligand-bridged M–M interactions [20, 27, 63, 64, 77]. In fact, by adding up the six $\delta(M\text{–}H)$ values for the bonding interactions, the three $\delta(M\cdots M)$ values for the non-bonding $M\cdots M$ interactions, the three $\delta(H\cdots H)$ values for the non-bonding $H\cdots H$ interactions, and the three $\delta(M\cdots H)$ values for the non-bonding $M\cdots H$ interactions in each M_3H_3 ring, a total of 3.042 (**4**), 3.303 (**5**), and 3.414 (**6**) electron pairs are obtained, which is approximately the same as if three localized M–M bonds, each one with a bond order of about unity, were present in each cluster.

Further insight into the delocalized nature of M–M bonding in clusters **4–6** may be appreciated from the electron localization function (ELF) [119–121]. The ELF of the hydride-bridged Mn complex **4** is depicted in Fig. 4 (representations of this function for complexes **1–6** are included in the Supplementary Material), which clearly shows a multicenter bonding between the M and H atoms (the function is clearly observed in the regions of the hydride ligands), as opposed to the more typical situation observed for the three binuclear compounds **1–3** [122].

Then, by summarizing all these features, it can be concluded that in clusters **4–6** there probably exists a multicenter *6c–6e* interaction involving the three metal atoms and the three hydrides.
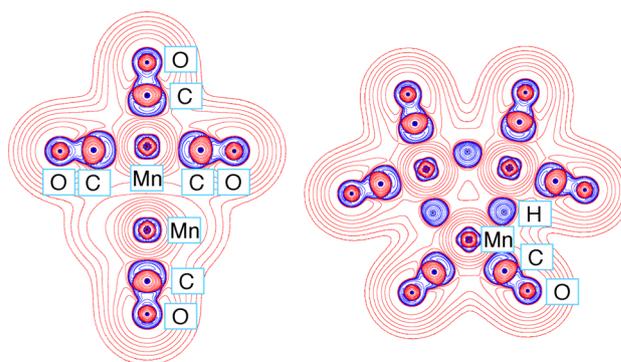
Fig. 4 Electron localization function (ELF) isosurface, at $\eta = 0.8$ e $Å^{-3}$, for complex **4**

Fig. 5 Laplacian of the electron density in relevant planes containing the metal atoms of complexes **1** (*left*) and **4** (*right*) (contour levels at 0.0 and $\pm (1,2,4,8) \times 10^n$ e $Å^{-5}$, with n ranging from +3 to –3). *Blue* and *red lines* represent negative and positive values, respectively

3.4 M–CO interactions in compounds 1–6

The topological indexes given in Table 2 for M–CO bonds in **1**–**6** are very similar to those found in the literature for other M–CO bonds [42–93]. These bonds are characterized by ρ_b values close to 1 e $Å^{-3}$ (higher than those of M–M and M–H bonds, but lower than those of pure covalent single bonds between nonmetal atoms), large positive values of $\nabla^2 \rho_b$ (much higher than those of M–M and M–H bonds), values of around unity for G_b/ρ_b (slightly higher than those of M–H bonds and more than twice those of M–M bonds), and small negative values for H_b/ρ_b (slightly more negative than those for both M–M and M–H bonds). In addition, a formal bond order of unity may be inferred from their δ(M–C) delocalization indexes.

Detecting π-back-donation from the metal to the CO ligand is difficult since the cylindrical symmetry of the density along a M–CO bond path hides any trace of preferential accumulation planes [64, 77]. Moreover, charges are sensitive to many different effects, like the polarity of the M–CO bond, and therefore cannot be taken as indicators of back-donation. The most reasonable sign of π-back-donation comes from the δ(M···O_{CO}) delocalization index, since π-back-donation involves significant M···O_{CO} interaction [20]. In fact, values of δ(Cu···O_{CO}) and δ(B···O_{CO}) in $[Cu(CO)_2]^+$ and H_3BCO, for which no π-back-donation exists, are very low, 0.09 and 0.04, respectively, whereas values of δ(M···O_{CO}) for Os, Ru, Fe, Co, and Ni carbonyl complexes are much higher, ranging from 0.15 to 0.25 [20, 64, 77]. The values of the δ(M···O_{CO}) index obtained for complexes **1**–**6** are precisely within this range (0.16, 0.15, 0.15, 0.18, 0.17, and 0.17, respectively), clearly indicating the presence of a significant π-back-donation, slightly higher in the trinuclear clusters than in the binuclear complexes.

Figure 5 is a representation of the Laplacian of the electron density in relevant planes of complexes **1** and **4**

(analogous representations for complexes **2**, **3**, **5**, and **6** are given in the Supplementary Information), which is useful to analyze M–M, M–H, and M–CO interactions. This figure shows that the valence shell charge depletion (VSCD) of each M atom has a nearly perfect cubic shape in compound **1** due to its octahedral coordination, although it is slightly deformed in cluster **4** due to the off-axis location of the bridging hydrido ligands. The valence shell charge concentrations (VSCCs) of H atoms in **4** are distorted toward the midpoint of each M–M edge, as has been previously found for other bridging H atoms [64, 77]. The key-lock mechanism prototypical of donor–acceptor interactions between a transition metal atom and a nonmetal atom is clearly appreciated here in all M–CO bonds. Each C atom points a VSCC directly toward a VSCD of its parent M atom, which also exhibits *trans* ligand-induced charge concentrations (also called ligand-opposed charge concentrations) in its valence shell. Other examples of this behavior have been found in compounds with alkyl ligands, for which the atomic graph of the metal atom in the Laplacian representation shows vertices (i.e., [3, –3] critical points for the Laplacian) that are opposite to a face (i.e., a region centered at a [3, +3] critical point for the Laplacian) linked to the ligand [10, 17, 18]. Additionally, a bond charge concentration, opposite to the M–M bond and pointing toward each axial coordination site, is also observed in the valence shells of the M atoms, a feature that may be fully appreciated in Figures S10–S15 of the Supplementary Information, where critical points of the Laplacian are depicted together with the contour lines.

4 Conclusions

Several local and integral topological properties of the electron density associated with the different interatomic

interactions present in the bi- and trinuclear group 7 transition metal complexes $[M_2(CO)_{10}]$ and $[M_3(\mu\text{-}H)_3(CO)_{12}]$ (M = Mn, Tc, Re) have been obtained using nonrelativistic and relativistic QTAIM calculations. A comparative analysis of these results has allowed the establishment of the following main conclusions:

(a) For the Mn compounds **1** and **4**, the results provided by the nonrelativistic calculations agree, both qualitatively and quantitatively, with those obtained using relativistic calculations, whereas for the Tc compounds **2** and **5**, relativistic corrections are small but significant (in this case, the scalar ZORA treatment was enough to provide accurate results). However, for the Re complexes **3** and **6**, the use of a fully relativistic spin–orbit hamiltonian was mandatory to achieve the same accuracy as that obtained for the Mn and Tc compounds, as indicated by the optimized geometries and atomic charges.

(b) The analysis of local and integral QTAIM topological indexes, in combination with the information obtained from the source function and the electron localization function, constitutes a useful method for studying and explaining M–M and M–ligand interactions.

(c) The presence of bridging hydrides considerably affects the electron density distribution of M–M interactions. In fact, the topological parameters of the unbridged M–M formal single bonds of **1**–**3** complexes, for which a localized bond has been identified, are very different from those of the H-bridged M–M interactions of **4**–**6**, for which a bond critical point (and the corresponding bond path) has not been found between the metal atoms.

(d) The contribution of the carbonyl ligands to the M–M bonding in the binuclear Re complex **3** is smaller than those in the Tc complex **2** and the Mn complex **1**. In addition, the metal atoms of **1**–**3** act as sinks for the electron density at the corresponding M–M *bcp*.

(e) The non-negligible values of delocalization indexes between the non-bonding interatomic interactions in the six-membered $M_3(\mu\text{-}H)_3$ rings of **4**–**6** clusters, as well as the ELF, suggest the existence of a delocalized kind of M–M interaction in these clusters. A multicenter 6c–6e interaction, involving the three metal atoms and the three hydrides of compounds **4**–**6**, is here proposed to explain the bonding in these clusters. It seems that the one-atom hydrido bridge that spans each M–M edge of these clusters is efficient enough to delocalize electronic density from the bridged M atoms.

(f) The calculated $\delta(M\cdots O_{CO})$ delocalization indexes suggest the existence of significant CO to M π-back-donation, which is slightly higher in the trinuclear clusters than in the binuclear complexes.

5 Supplementary Material

Atomic coordinates for the theoretically optimized geometries of complexes **1**–**6**, further topological properties obtained from relativistic and nonrelativistic calculations, and complementary images of the graphical representations provided in Figs. 2–5.

References

1. Bader RFW (1990) Atoms in molecules: a quantum theory. Clarendon Press, Oxford
2. Popelier PLA (2000) Atoms in molecules: an introduction. Prentice Hall, Harlow
3. Coppens P (1997) X-ray charge densities and chemical bonding. International Union of Crystallography and Oxford University Press, Oxford
4. Matta CF, Boyd RJ (eds) (2007) The quantum theory of atoms in molecules. Wiley-VCH, Weinheim
5. Gatti C, Macchi P (eds) (2012) Modern charge density analysis. Springer, Heidelberg
6. Foroutan-Nejad C, Shahbazian S, Marek R (2014) Chem Eur J 20:10140–10152
7. Macchi P (2013) Crystallogr Rev 19:58–101
8. Macchi P, Gillet JM, Taulelle F, Campo J, Claisere N, Lecomte C (2015) IUCr J 2:441–451
9. Bader RFW (1998) J Phys Chem A 102:7314–7323
10. Cortés-Guzmán F, Bader RFW (2005) Coord Chem Rev 249:633–662
11. Koritsanszky TS, Coppens P (2001) Chem Rev 101:1583–1627
12. Gatti C (2005) Z Kristallogr 220:399–457
13. Coppens P, Iversen BB, Larsen FK (2005) Coord Chem Rev 249:179–195
14. Ling Y, Zhang Y (2010) Ann Rep Comput Chem 6:65–77
15. Macchi P (2009) Angew Chem Int Ed 48:5793–5795
16. Bader RFW, Stephens ME (1975) J Am Chem Soc 97:7391–7399
17. Byteway I, Gillespie RJ, Tang TH, Bader RFW (1995) Inorg Chem 34:2407–2414
18. Scherer W, Sirsch P, Shorokhov D, Tafipolsky M, McGrady GS, Gullo E (2003) Chem Eur J 9:6057–6070
19. Jørgensen MRV, Hathwar VR, Bindzus N, Wahlberg N, Chen YS, Overgaard J, Iversen BB (2014) IUCr J 1:267–280
20. Macchi P, Sironi A (2003) Coord Chem Rev 238:383–412
21. Farrugia LJ, Evans C, Tegel M (2006) J Phys Chem A 110:7952–7961
22. Farrugia LJ, Evans C, Lentz D, Roemer M (2009) J Am Chem Soc 131:1251–1268
23. Van der Maelen JF, Gutiérrez-Puebla E, Monge A, García-Granda S, Resa I, Carmona E, Fernández-Díaz MT, McIntyre GJ, Pattison P, Weber HP (2007) Acta Crystallogr B 63:862–868
24. Macchi P, Proserpio DM, Sironi A (1998) J Am Chem Soc 120:13429–13435
25. Overgaard J, Clausen HF, Platts JA, Iversen BB (2008) J Am Chem Soc 130:3834–3843
26. Macchi P, Garlaschelli L, Sironi A (2002) J Am Chem Soc 124:14173–14184

27. Bo C, Sarasa JP, Poblet JM (1993) J Phys Chem 97:6362–6366
28. Low AA, Kunze KL, MacDougall PJ, Hall MB (1991) Inorg Chem 30:1079–1086
29. Bianchi R, Gervasio G, Marabello D (2000) Inorg Chem 39:2360–2366
30. Van der Maelen JF, Ruiz J, García-Granda S (2005) J Theor Comput Chem 4:823–832
31. Wolstenholme DJ, Traboulsee KT, Decken A, McGrady GS (2010) Organometallics 29:5769–5772
32. Popov AA, Dunsch L (2009) Chem Eur J 15:9707–9729
33. Varadwaj PR, Marques HM (2010) Theor Chem Acc 127:711–725
34. Reisinger A, Trapp N, Krossing I, Altmannshofer S, Herz V, Presnitz M, Scherer W (2007) Angew Chem Int Ed 46:8295–8298
35. Himmel D, Trapp N, Krossing I, Altmannshofer S, Herz V, Eickerling G, Scherer W (2008) Angew Chem Int Ed 47:7798–7801
36. Poulsen RD, Bentien A, Chevalier M, Iversen BB (2005) J Am Chem Soc 127:9156–9166
37. Abramov YA, Brammer L, Klooster WT, Bullock RM (1998) Inorg Chem 37:6317–6328
38. Batool M, Martin TA, Algarra AG, George MW, Macgregor SA, Mahon MF, Whittlesey MK (2012) Organometallics 31:4971–4979
39. Nuss H, Claiser N, Pillet S, Lugan N, Despagnet-Ayoub E, Etienne M, Lecomte C (2012) Dalton Trans 41:6598–6601
40. Gagliardi L (2014) In: Frenking G, Shaik S (eds) The chemical bond: chemical bonding across the periodic table. Wiley-VCH, Weinheim, pp 253–268
41. Merino G, Donald KJ, D'Acchioli JS, Hoffmann R (2007) J Am Chem Soc 129:15295–15302
42. Nguyen T, Sutton AD, Brynda M, Fettinger JC, Long GJ, Power PP (2005) Science 310:844–847
43. La Macchia G, Li Manni G, Todorova TK, Brynda M, Aquilante F, Roos BO, Gagliardi L (2010) Inorg Chem 49:5216–5222
44. Brynda M, Gagliardi L, Roos BO (2009) Chem Phys Lett 471:1–10
45. Kreisel KA, Yap GPA, Dmitrenko O, Landis CR, Theopold KH (2007) J Am Chem Soc 129:14162–14163
46. Noor A, Wagner FR, Kempe R (2008) Angew Chem Int Ed 47:7246–7249
47. Tsai YC, Hsu CW, Yu JSK, Lee GH, Wang Y, Kuo TS (2008) Angew Chem Int Ed 47:7250–7253
48. Hsu CW, Yu JSK, Yen CH, Lee GH, Wang Y, Tsai YC (2008) Angew Chem Int Ed 47:9933–9936
49. Horvath S, Gorelsky SI, Gambarotta S, Korobkov I (2008) Angew Chem Int Ed 47:9937–9940
50. Weinhold F, Landis CR (2007) Science 316:61–63
51. Wagner FR, Noor A, Kempe R (2009) Nat Chem 1:529–536
52. Hall MB (1980) J Am Chem Soc 102:2104–2106
53. Kok RA, Hall MB (1983) Inorg Chem 22:728–734
54. Chisholm MN, Davidson ER, Huffmann JC, Quinlan KB (2001) J Am Chem Soc 123:9652–9664
55. Chisholm MN, Davidson ER, Quinlan KB (2002) J Am Chem Soc 124:15351–15358
56. Connor JA, Pilcher G, Skinner HA, Chisholm MH, Cotton FA (1978) J Am Chem Soc 100:7738–7739
57. Gagliardi L, Roos BO (2003) Inorg Chem 42:1599–1603
58. Saito K, Nakao Y, Sato H, Sakaki S (2006) J Phys Chem A 110:9710–9717
59. Roos BO, Borin AC, Gagliardi L (2007) Angew Chem Int Ed 46:1469–1472
60. Brown DA, Chambers WJ, Fitzpatrick NJ, Rawlinson SRM (1971) J Chem Soc A 720–725
61. Rosa A, Ricciardi G, Baerends EJ, Stufkens DJ (1995) Inorg Chem 34:3425–3432
62. Weck PF, Sergeeva AP, Kim E, Boldyrev AI, Czerwinski KR (2011) Inorg Chem 50:1039–1046
63. Gatti C, Lasi D (2007) Faraday Discuss 135:55–78
64. Van der Maelen JF, García-Granda S, Cabeza JA (2011) Comput Theor Chem 968:55–63
65. Llusar R, Beltrán A, Andrés J, Fuster F, Silvi B (2001) J Phys Chem A 105:9460–9466
66. Farrugia LJ, Senn HM (2010) J Phys Chem A 114:13418–13433
67. Farrugia LJ, Macchi P (2012) Struct Bonding 146:127–158
68. Van der Maelen JF, Cabeza JA (2012) Inorg Chem 51:7384–7391
69. Macchi P, Krawczuk A (2015) Comput Theor Chem 1053:165–172
70. Gatti C (2013) Phys Scrip 87:048102
71. Curado N, Carrasco M, Álvarez E, Maya C, Peloso R, Rodríguez A, López-Serrano J, Carmona E (2015) J Am Chem Soc 137:12378–12387
72. Gervasio G, Bianchi R, Marabello D (2005) Chem Phys Lett 407:18–22
73. Macchi P, Garlaschelli L, Martinengo S, Sironi A (1999) J Am Chem Soc 121:10428–10429
74. Feliz M, Llusar R, Andrés J, Berski S, Silvi B (2002) New J Chem 26:844–850
75. Byteway I, Griffith CS, Koutsantonis GA, Skelton BW, White AH (2007) Eur J Inorg Chem 3240–3246
76. Niskanen M, Hirva P, Haukka M (2009) J Chem Theory Comput 5:1084–1090
77. Cabeza JA, Van der Maelen JF, García-Granda S (2009) Organometallics 28:3666–3672
78. Gervasio G, Marabello D, Bianchi R, Forni A (2010) J Phys Chem A 114:9368–9373
79. Dinda S, Samuelson AG (2012) Chem Eur J 18:3032–3042
80. Farrugia LJ, Evans C, Senn HM, Aänninen MM, Sillanpää R (2012) Organometallics 31:2559–2570
81. Bianchi R, Gervasio G, Marabello D (1998) Chem Commun 1535–1536
82. Ponec R, Yuzhakov G, Sundberg MR (2005) J Comput Chem 26:447–454
83. Ponec R, Yuzhakov G (2007) Theor Chem Acc 118:791–797
84. Bertini L, Fantucci G, De Gioia L (2011) Organometallics 30:487–498
85. Flierler U, Burzler M, Leusser D, Henn J, Ott H, Braunschweig H, Stalke D (2008) Angew Chem Int Ed 47:4321–4325
86. Götz K, Kaupp M, Braunschweig H, Stalke D (2009) Chem Eur J 15:623–632
87. Ponec R (2015) Comput Theor Chem 1053:195–213
88. Wu LC, Hsu CW, Chuang YC, Lee GH, Tsai YC, Wang Y (2011) J Phys Chem A 115:12602–12615
89. Gatti C (2012) Struct & Bonding 147:193–286
90. Macchi P, Donghi D, Sironi A (2005) J Am Chem Soc 127:16494–16504
91. Foroutan-Nejad C, Vicha J, Marek R, Patzschke M (2015) Phys Chem Chem Phys 17:24182–24192
92. Li X, Huo S, Zeng Y, Sun Z, Zheng S, Meng L (2013) Organometallics 32:1060–1066
93. Bertolotti F, Forni A, Gervasio G, Marabello D, Diana E (2012) Polyhedron 42:118–127
94. Eickerling G, Mastalerz R, Herz V, Scherer W, Himmel HJ, Reiher M (2007) J Chem Theory Comput 3:2182–2197
95. Eickerling G, Reiher M (2008) J Chem Theory Comput 4:286–296
96. Hebben N, Himmel HJ, Eickerling G, Hermann C, Reiher M, Herz V, Presnitz M, Scherer W (2007) Chem Eur J 13:10078–10087

97. Reiher M, Wolf A (2009) Relativistic quantum chemistry: the fundamental theory of molecular science. Wiley-VCH, Weinheim

98. Fux S, Reiher M (2012) Struct Bonding 147:99–142

99. Ponec R, Bučinský L, Gatti C (2010) J Chem Theory Comput 6:3113–3121

100. Sablon N, Mastalerz R, De Proft F, Geerlings P, Reiher M (2010) Theor Chem Acc 127:195–202

101. Schwerdtfeger P (2014) In: Frenking G, Shaik S (eds) The chemical bond: fundamental aspects of chemical bonding. Wiley-VCH, Weinheim, Germany, pp 383–404

102. Frisch MJ, Trucks GW, Schlegel HB, Scuseria GE, Robb MA, Cheeseman JR, Scalmani G, Barone V, Mennucci B, Petersson GA, Nakatsuji H, Caricato M, Li X, Hratchian HP, Izmaylov AF, Bloino J, Zheng G, Sonnenberg JL, Hada M, Ehara M, Toyota K, Fukuda R, Hasegawa J, Ishida M, Nakajima T, Honda Y, Kitao O, Nakai H, Vreven T, Montgomery JA Jr, Peralta JE, Ogliaro F, Bearpark M, Heyd JJ, Brothers E, Kudin KN, Staroverov VN, Keith T, Kobayashi R, Normand J, Raghavachari K, Rendell A, Burant JC, Iyengar SS, Tomasi J, Cossi M, Rega N, Millam JM, Klene M, Knox JE, Cross JB, Bakken V, Adamo C, Jaramillo J, Gomperts R, Stratmann RE, Yazyev O, Austin AJ, Cammi R, Pomelli C, Ochterski JW, Martin RL, Morokuma K, Zakrzewski VG, Voth GA, Salvador P, Dannenberg JJ, Dapprich S, Daniels AD, Farkas O, Foresman JB, Ortiz JV, Cioslowski J, Fox DJ (2010) GAUSSIAN09, Revision B.01. Gaussian Inc., Wallingford, CT

103. Lee C, Yang W, Parr RG (1988) Phys Rev B 37:785–789

104. Perdew JP (1986) Phys Rev B 33:8822–8824

105. Becke AD (1993) J Chem Phys 98:5648–5652

106. Huzinaga S, Miguel B (1990) Chem Phys Lett 175:289–291

107. Huzinaga S, Klobukowski M (1993) Chem Phys Lett 212:260–264

108. van Lenthe E, Baerends EJ (2003) J Comput Chem 24:1142–1156

109. Baerends EJ, Ziegler T, Autschbach J, Bashford D, Bérces A, Bickelhaupt FM, Bo C, Boerrigter PM, Cavallo L, Chong DP, Deng L, Dickson RM, Ellis DE, van Faassen M, Fan L, Fischer TH, Fonseca-Guerra C, Ghysels A, Giammona A, van Gisbergen SJA, Götz AW, Groeneveld JA, Gritsenko OV, Grüning M, Gusarov S, Harris FE, van den Hoek P, Jacob CR, Jacobsen H, Jensen L, Kaminski JW, van Kessel G, Kootstra F, Kovalenko A, Krykunov MV, van Lenthe E, McCormack DA, Michalak A, Mitoraj M, Neugebauer J, Nicu VP, Noodleman L, Osinga VP, Patchkovskii S, Philipsen PHT, Post D, Pye CC, Ravenek W, Rodríguez JI, Ros P, Schipper PRT, Schreckenbach G, Seldenthuis JS, Seth M, Snijders JG, Solà M, Swart M, Swerhone D, te Velde G, Vernooijs P, Versluis L, Visscher L, Visser O, Wang F, Wesolowski TA, van Wezenbeek EM, Wiesenekker G, Wolff SK, Woo TK, Yakovlev AL (2012) ADF2012, Revision 01d, SCM, Theoretical Chemistry. Vrije Universiteit, Amsterdam

110. Farrugia LJ, Mallinson PR, Stewart B (2003) Acta Crystallogr B 59:234–247

111. Bailey MF, Dahl LF (1965) Inorg Chem 4:1140–1145

112. Churchill MR, Amoh KN, Wasserman HJ (1981) Inorg Chem 20:1609–1611

113. Kirtley SW, Olsen JP, Bau R (1973) J Am Chem Soc 95:4532–4536

114. Alberto R, Schibli R, Schubiger A, Abram U, Hübener R, Berke H, Kaden TA (1996) Chem Commun 1291–1292

115. Masciocchi N, Sironi A (1990) J Am Chem Soc 112:9395–9397

116. Keith TA (2015) AIMAll, Version 15.09.27, TK Gristmill Software, Overland Park, Kansas

117. Biegler-König F, Schönbohm J (2002) J Comput Chem 23:1489–1494

118. Kohout M (2011) DGrid 4.6. Max Planck Institute for Physical Chemistry of Solids, Dresden

119. Matito E, Solá M (2009) Coord Chem Rev 253:647–665

120. Grin Y, Savin A, Silvi B (2014) In: Frenking G, Shaik S (eds) The chemical bond: fundamental aspects of chemical bonding. Wiley-VCH, Weinheim, pp 345–382

121. Feixas F, Matito E, Duran M, Poater J, Solà M (2011) Theor Chem Acc 128:419–431

122. Kohout M, Wagner FR, Grin Y (2002) Theor Chem Acc 108:150–156